Lagrangian coherent structures from approximate velocity data

G. Haller
Department of Mechanical Engineering, Massachusetts Institute of Technology, Cambridge, Massachusetts 02139

(Received 6 September 2001; accepted 20 March 2002; published 2 May 2002)

This paper examines whether hyperbolic Lagrangian structures—such as stable and unstable manifolds—found in model velocity data represent reliable predictions for mixing in the true fluid velocity field. The error between the model and the true velocity field may result from velocity interpolation, extrapolation, measurement imprecisions, or any other deterministic source. We find that even large velocity errors lead to reliable predictions on Lagrangian coherent structures, as long as the errors remain small in a special time-weighted norm. More specifically, we show how model predictions from the Okubo–Weiss criterion or from finite-time Lyapunov exponents can be validated. We also estimate how close the true Lagrangian coherent structures are to those predicted by models. © *2002 American Institute of Physics.* [DOI: 10.1063/1.1477449]

I. INTRODUCTION

Two-dimensional chaotic advection in time-periodic fluid velocity fields is closely associated with the presence of invariant manifolds.[1] For the period-one map, or Poincaré map, these manifolds appear as stable and unstable manifolds of hyperbolic fixed points. Unstable manifolds act as attracting material lines that create global folding patterns for passive tracers; stable manifolds act as repelling material lines that are responsible for stretching of tracer blobs. Advective mixing is therefore governed by stable and unstable manifolds, or in other words, *hyperbolic material lines*.

Recent progress in nonlinear dynamics has extended the above picture to velocity fields with aperiodic or even turbulent time dependence. While no Poincaré maps are available in this context, families of hyperbolic material lines continue to organize tracer mixing. These families are formed by finite-time stable and unstable manifolds of special (nonperiodic) fluid trajectories.[2,3] Several algorithms for the extraction of such hyperbolic material lines have been proposed, with a notable emphasis on geophysical applications.[4–12]

Although the extraction algorithms have performed well on interpolated two-dimensional velocity data, the effect of data processing and measurement errors on the result has remained unclear. When performed with care, data processing, such as velocity interpolation or extrapolation, provides a velocity field that is arguably close to the true field. Similarly, careful experimental techniques lead to a data set that is close to the true velocity field. Closeness in the Eulerian sense, however, does not imply closeness in the Lagrangian sense. Indeed, local errors in the calculation of fluid trajectories will accumulate and lead to growing errors in particle positions. Because all known methods for locating hyperbolic material lines use particle positions, one has to contend with large errors or even spurious structures that are artifacts of the processing techniques. Classic dynamical systems estimates only reinforce one's concerns: They indicate exponential separation between Lagrangian truth and its approximation. Another dynamical systems principle, the robustness of hyperbolic sets under small enough perturbations, offers no help in practical examples where velocity errors typically lie outside the range of perturbation theory.

This paper will provide general estimates for the accuracy of invariant manifold reconstruction from velocity models. By a model velocity field, we simply mean a time-dependent data set that one obtains after refining some numerical or experimental velocity data. The difference between the true and model velocity fields may result from this refinement, as well as from additional deterministic errors in data generation and data acquisition.

We show that as long as the model and the true velocity field are close in a time-weighted norm $\|\cdot\|_w$, a hyperbolic material line of the model data set signals a hyperbolic material line in the true flow. To evaluate our closeness criteria, one needs to estimate the attraction or repulsion rate of the model material line, and the magnitude of the velocity error. We give two different formulations, with different ways of estimating the attraction and repulsion rates. Our first result, Theorem 1, uses rates inferred from a Lagrangian Okubo–Weiss criterion,[2] while our second result, Theorem 2, uses rates obtained from a direct Lyapunov exponent calculation.[7]

The main lessons from our analysis are independent of the invariant manifold extraction method, and can be summarized as follows. First, even large modeling errors are admissible, if they are localized in time. Large errors are also admissible if the hyperbolic material line found in the model attracts or repels strongly enough, or its time of existence is long enough. These conclusions follow because the weight function in the norm $\|\cdot\|_w$ turns out to decay exponentially in time (see Fig. 1).

Second, true and model trajectories may separate exponentially, but true and model hyperbolic material lines will not. In other words, errors in individual particle paths will spread *along* hyperbolic material lines; errors transverse to hyperbolic material lines remain small (see Fig. 2).

Third, maximizing curves of particle separation plots (such as relative dispersion, finite-time or finite-size

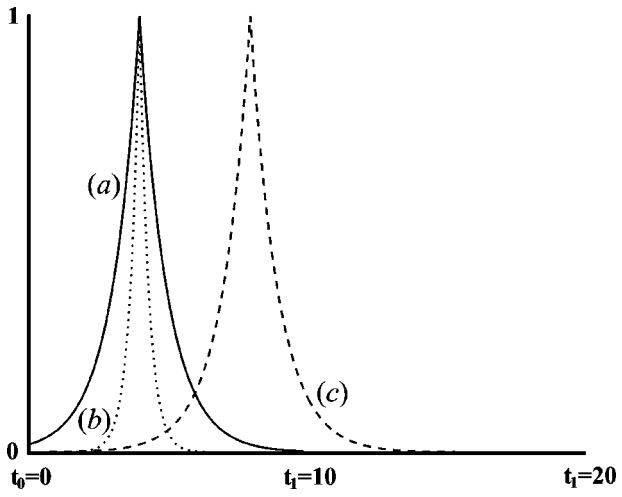

FIG. 1. The graph of the weight function $w_t(\tau)$ for the norm $\|\cdot\|_w = \max_{t\in[t_0,t_1]}\int_{t_0}^{t_1}|\cdot|\, w_t(\tau)\, dt$, in which the modeling error must be small for good predictions on hyperbolic material lines. The peak value $w_t(\tau)$ is always at $\tau=t$. (a) $w_t(\tau)$ with $t=4$ for a typical hyperbolic material line of the model velocity data over the time interval [0,10]. (b) $w_t(\tau)$ with $t=4$ for a strongly hyperbolic material line (c) $w_t(\tau)$ with $t=8$ for a material line with a longer interval of hyperbolicity.

Lyapunov exponent plots) are hyperbolic material lines if and only if the Lagrangian rate of strain is nonzero along them. This result enables one to distinguish hyperbolic material lines from lines of high shear in particle separation plots (see Example 3 of Sec. VI).

To establish the above conclusions, we use a finite-time invariant manifold approach.[2] Along a candidate trajectory, we select a coordinate frame in which stretching and compression separate at leading order. Working in this frame, we construct repelling and attracting material lines as finite-time hyperbolic invariant manifolds. In our arguments, the interpolation error does not need to be continuous in time, but it has to be Lipschitz continuous in space. Accordingly, the hyperbolic material lines we locate are Lipschitz in space and continuous in time.

The organization of this paper is as follows. In Sec. II we fix notation. Section III contains our first result on the admissible modeling error and on the accuracy of invariant manifolds for the Lagrangian Okubo–Weiss criterion. Section IV gives a similar result for manifolds obtained from finite-time Lyapunov exponent calculations. Section V briefly explains how our theorems can validate invariant manifold predictions by other Lagrangian diagnostic tools, such as finite-size Lyapunov exponents, relative or absolute dispersion, and entropy. Section VI offers simple examples that demonstrate the use of our criteria in applications. A summary and a list of open problems conclude the paper in Sec. VII. We enclose the proofs of our theorems in the Appendix.

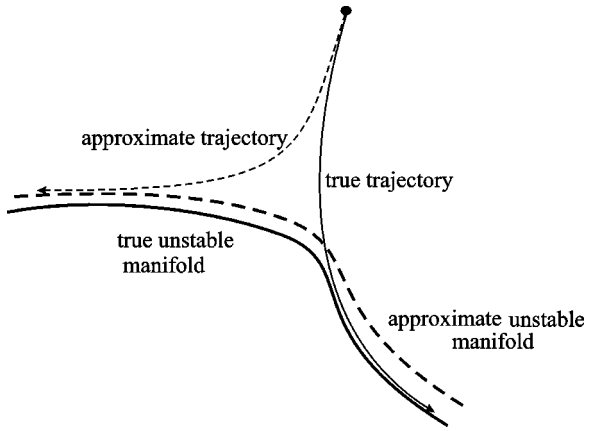

FIG. 2. Schematic relationship between modeled and true attracting material lines (finite-time unstable manifolds). Note that, unlike hyperbolic material lines, modeled and true trajectories will generally separate exponentially.

II. NOTATION AND DEFINITIONS

Consider a two-dimensional velocity field

$$\dot{\mathbf{x}}=\mathbf{v}(\mathbf{x},t)=\mathbf{u}(\mathbf{x},t)+\boldsymbol{\mu}(\mathbf{x},t), \tag{1}$$

where $\mathbf{v}(\mathbf{x},t)$ denotes the true velocity field, $\mathbf{u}$ is the model velocity field that one intends to use for Lagrangian data analysis, and $\boldsymbol{\mu}(\mathbf{x},t)$ is the modeling error. In this paper $\boldsymbol{\mu}$ is assumed to be a deterministic function that may arise from interpolating $\mathbf{v}$ between gridpoints, from extrapolating $\mathbf{v}$ to unknown domains or boundary points, or from errors in velocity measurement. In all our arguments, the spatial variable $\mathbf{x}$ is taken from a bounded domain D, and the model field $\mathbf{u}$ is defined over a finite time interval $\mathcal{I}$.

We assume that the model velocity $\mathbf{u}$ is twice continuously differentiable in space, and its second derivative obeys the bound

$$|\nabla^2\mathbf{u}(\mathbf{x},t)|\leqslant C, \tag{2}$$

for some nonnegative constant C. We further assume that $\boldsymbol{\mu}(\mathbf{x},t)$ satisfies

$$|\boldsymbol{\mu}(\mathbf{x},t)|\leqslant B(t), \quad |\boldsymbol{\mu}(\mathbf{x},t)-\boldsymbol{\mu}(\tilde{\mathbf{x}},t)|\leqslant L(t)|\mathbf{x}-\tilde{\mathbf{x}}|, \tag{3}$$

for all $\mathbf{x}$, $\bar{\mathbf{x}}\in D$ and $t\in\mathcal{I}$. In other words, we assume that $\boldsymbol{\mu}$ is bounded and Lipschitz in $\mathbf{x}$ with Lipschitz constant $L(t)$. Note that we allow $\boldsymbol{\mu}$ to jump in time at any spatial location within D. Finally, we assume that a trajectory $\bar{\mathbf{x}}(t)$ of the model velocity field $\mathbf{u}(\mathbf{x},t)$ is known

$$\frac{d}{dt}\bar{\mathbf{x}}(t)=\mathbf{u}(\bar{\mathbf{x}}(t),t).$$

To fix terminology, we recall that a material line of this velocity field is a continuous time-dependent curve $\mathcal{M}(t)$ advected by the model flow. We call $\mathcal{M}(t)$ a *repelling material line* over a time interval I if infinitesimal perturbations off this line grow monotonically under the linearized flow.[3] We call $\mathcal{M}(t)$ an *attracting material line* over I if it is a repelling material line over I in backward time. (For example, the local stable manifold of a fixed point p of a Poincaré map is a repelling material line over any finite time interval.) We refer to attracting and repelling material lines jointly as *hyperbolic material lines*.

III. LAGRANGIAN STRUCTURES FROM THE OKUBO–WEISS CRITERION

The gradient of $\mathbf{u}$ along $\overline{\mathbf{x}}(t)$ is given by the time-dependent matrix $\nabla\mathbf{u}(\overline{\mathbf{x}}(t),t)$. We assume that over some finite time interval $I=[t_0,t_1]$ within $\mathcal{I}$, we have

$$\det\nabla\mathbf{u}(\overline{\mathbf{x}}(t),t)<0, \tag{4}$$

which implies that $\nabla\mathbf{u}(\overline{\mathbf{x}}(t),t)$ has real eigenvalues

$$-\lambda_1(t)<0<\lambda_2(t). \tag{5}$$

We recall that Okubo[13] and Weiss[14] identify the spatial region satisfying $\det\nabla\mathbf{u}(\mathbf{x},t)<0$ as hyperbolic. Here hyperbolicity is meant in an instantaneous Eulerian sense; Lagrangian hyperbolicity of $\overline{\mathbf{x}}(t)$ would only follow if $\overline{\mathbf{x}}(t)$ were a fixed point and $\mathbf{u}$ were a steady velocity field.

We seek to answer the following question: Under what conditions does $\overline{\mathbf{x}}(t)$, a model trajectory staying in the Okubo–Weiss hyperbolic region, indicate the existence of nearby hyperbolic material lines in the true flow? We start by defining the quantities

$$\lambda_{k\,\min}=\min_{t\in I}\lambda_k(t),\quad k=1,2,\quad \lambda_{\min}=\min(\lambda_{1\,\min},\lambda_{2\,\min}), \tag{6}$$

which measure the minimum of the norm of the eigenvalues $\lambda_k(t)$. We also define the eigenvectors $\mathbf{e}_1(t)$ and $\mathbf{e}_2(t)$ corresponding to $-\lambda_1(t)$ and $\lambda_2(t)$, and assume that they are normalized to $|\mathbf{e}_k(t)|=1$, and are chosen such that $\mathbf{e}_k(t)$ depends smoothly on t. Using the matrix of eigenvectors $\mathbf{T}(t)=[\mathbf{e}_1(t),\mathbf{e}_2(t)]$, we define the two quantities

$$\alpha=\min_{t\in I}|\det\mathbf{T}(t)|,\quad \beta=\max_{t\in I}\|\dot{\mathbf{T}}(t)\|, \tag{7}$$

with $\|\dot{\mathbf{T}}\|=\sqrt{\Sigma_{i,j}\dot{T}_{ij}^2}$ denoting the norm of the matrix $\dot{\mathbf{T}}$. Note that α is a measure of the minimal angle between the two eigenvectors, while β measures the maximal rate at which the eigenvectors change.

As it turns out below, it is not the actual error, but rather its weighted norm along the model trajectory $\overline{\mathbf{x}}(t)$ that affects the existence of Lagrangian structures in the true data set. The weight function we obtain in our mathematical arguments is

$$w_t(\tau)=\begin{cases} e^{-\int_\tau^t\lambda_1(s)ds} & \text{if}\quad \tau\in[t_0,t) \\ e^{-\int_t^\tau\lambda_2(s)ds} & \text{if}\quad \tau\in[t,t_1] \end{cases}, \tag{8}$$

where the time parameter t is taken from the interval $I=[t_0,t_1]$. For a typical shape of $w_t(\tau)$, we refer the reader back to Fig. 1. Using $w_t(\tau)$, we define two measures of the modeling error

$$B_w=\max_{t\in I}\int_{t_0}^{t_1}B(\tau)w_t(\tau)\,d\tau,$$

$$L_w=\max_{t\in I}\int_{t_0}^{t_1}L(\tau)w_t(\tau)\,d\tau.$$

Note that a large spike in the error will still be small in terms of these measures, as long as its duration is short. Also note that along a trajectory with larger λ_k, the same Eulerian error will produce smaller B_w and L_w values.

Finally, we define the distance

$$\Delta=\begin{cases} \dfrac{\alpha\lambda_{\min}-2\sqrt{2}\beta}{2\sqrt{2}C} & \text{if}\quad C>0 \\ \dfrac{2\lambda_{\min}}{\alpha\lambda_{\min}-2\sqrt{2}\beta} & \text{if}\quad C=0 \end{cases}, \tag{9}$$

for use in our main theorem. Note that $C=0$ arises for linear model velocity fields. We include the linear case in our discussion for completeness, and for use in our later examples.

Theorem 1: *Suppose that along a trajectory* $\overline{\mathbf{x}}(t)$ *of the model velocity field* $\mathbf{u}$, *condition* (4) *is satisfied. Assume further that*

$$\lambda_{\min}>2\sqrt{2}\,\frac{\beta}{\alpha},\quad B_wC<\frac{(\alpha\lambda_{\min}-2\sqrt{2}\beta)^2}{8\lambda_{\min}}, \tag{10}$$

and

$$L_w<\frac{\alpha\lambda_{\min}-2\sqrt{2}\beta}{2\sqrt{2}\lambda_{\min}}. \tag{11}$$

Then

(i) *the model trajectory* $\overline{\mathbf{x}}(t)$ *is contained in a hyperbolic material line* $\mathcal{M}(t)$ *over the time interval I;*

(ii) *the true velocity field* $\mathbf{v}(\mathbf{x},t)$ *admits a hyperbolic material line* $\mathcal{N}(t)$ *which is at least* Δ*-close to* $\mathcal{M}(t)$ *near the trajectory* $\overline{\mathbf{x}}(t)$.

We will prove Theorem 1 in Appendix A.

IV. LAGRANGIAN STRUCTURES FROM FINITE-TIME LYAPUNOV EXPONENTS

We now move on to discuss the relevance of finite-time Lyapunov exponent calculations on the model field for the true velocity field $\mathbf{v}$. Let $\mathbf{F}^t(\mathbf{x}_0)$ denote the current position of the fluid trajectory that started from the point $\mathbf{x}_0$ at time t_0. We again fix a particular trajectory $\overline{\mathbf{x}}(t)=\mathbf{F}^t(\mathbf{x}_0)$ of the model velocity field $\mathbf{u}$ over the time interval $I=[t_0,t_1]$.

Infinitesimal perturbations to $\overline{\mathbf{x}}(t)$ satisfy the equation

$$\dot{\boldsymbol{\xi}}=\nabla\mathbf{u}(\overline{\mathbf{x}}(t),t)\boldsymbol{\xi}, \tag{12}$$

which admits the solution

$$\boldsymbol{\xi}(t)=\nabla\mathbf{F}^t(\mathbf{x}_0)\boldsymbol{\xi}_0.$$

Assuming that $\nabla\mathbf{F}^t(\mathbf{x}_0)$ is known for any $t\in I$, we define the time-dependent scalar field

$$\sigma_t(\mathbf{x}_0)=\lambda_{\max}([\nabla\mathbf{F}^t(\mathbf{x}_0)]^*\nabla\mathbf{F}^t(\mathbf{x}_0)), \tag{13}$$

the maximal eigenvalue of the Cauchy–Green strain tensor field $[\nabla\mathbf{F}^t(\mathbf{x}_0)]^*\nabla\mathbf{F}^t(\mathbf{x}_0)$. (Here * refers to matrix transposition and $\lambda_{\max}(\mathbf{A})$ denotes the maximal eigenvalue of a matrix $\mathbf{A}$.) Note that $\sqrt{\sigma_t(\mathbf{x}_0)}$ gives the maximal stretch that

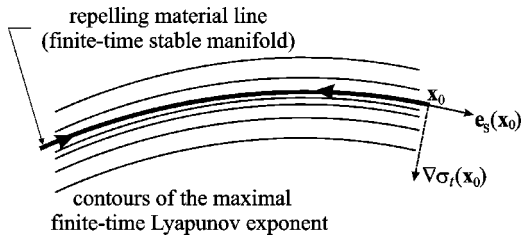

FIG. 3. The choice of the unit vector $\mathbf{e}_s(\mathbf{x}_0)$.

solutions of (12) will experience over the time interval $[t_0,t]$. As argued by Haller,[7] hyperbolic material lines at $t=t_0$ tend to be local maximizing curves of $\sigma_t(\mathbf{x}_0)$. To avoid deriving extra conditions that exclude special degenerate cases, we shall simply assert that finite-time hyperbolic material lines are local maximizing curves of the $\sigma_t(\mathbf{x}_0)$, i.e., the value of σ_t is nonincreasing in directions normal to these material lines. We require ''nonincreasing'' instead of ''decreasing'' because no finite-time hyperbolic material line can be locally unique.[2]

To illuminate the meaning of σ_t further, we recall that

$$\mathrm{DLE}_t(\mathbf{x}_0)=\frac{1}{2(t-t_0)}\log\sigma_t(\mathbf{x}_0),$$

is just the maximal *direct finite-time Lyapunov exponent* (DLE) associated with the trajectory $\overline{\mathbf{x}}(t)$. In this context, ''direct'' means the exponent is computed directly from its definition, i.e., from differentiating fluid trajectories with respect to their initial positions. Contour plots of $\mathrm{DLE}_t(\mathbf{x}_0)$ usually reveal more local maximizers of stretching than that of $\sigma_t(\mathbf{x}_0)$; this is why the DLE field is typically better suited for Lagrangian data analysis than the $\sigma_t(\mathbf{x}_0)$ field.

We now use the DLE field to infer the location of hyperbolic material lines in the flow. We start by selecting a unit vector $\mathbf{e}_s$ based at the initial position $\mathbf{x}_0$. This unit vector will be a candidate for a tangent vector to the $t=t_0$ section of a repelling material line containing $\overline{\mathbf{x}}(t)$. As follows from Ref. 7, if t_1-t_0 is large enough then a good choice for $\mathbf{e}_s$ is given by

$$\mathbf{e}_s(\mathbf{x}_0)=\frac{\nabla\sigma_{t_1}(\mathbf{x}_0)^\perp}{|\nabla\sigma_{t_1}(\mathbf{x}_0)^\perp|},\tag{14}$$

i.e., by a unit vector tangent to the contour curve of $\sigma_{t_1}(\mathbf{x}_0)$ passing through $\mathbf{x}_0$. (Here $\mathbf{a}^\perp$ denotes a vector normal to the vector $\mathbf{a}$ with $|\mathbf{a}^\perp|=|\mathbf{a}|$.) Shown in Fig. 3, this choice for $\mathbf{e}_s$ is motivated by the observation that $\sigma_t(\mathbf{x}_0)$ admits a ridge along the $t=t_0$ slice of the locally strongest repelling material line.

If the point $\mathbf{x}_0$ is contained in such a ridge, $\nabla\sigma_t(\mathbf{x}_0)^\perp/|\nabla\sigma_t(\mathbf{x}_0)|$ will produce a unit vector that is approximately tangent to the ridge (see Fig. 4 for a numerical example). As Fig. 4 shows, formula (14) indeed produces correctly oriented tangent vectors for the strongest repelling material lines. For weaker lines, more refined choices of $\mathbf{e}_s$ may work better.

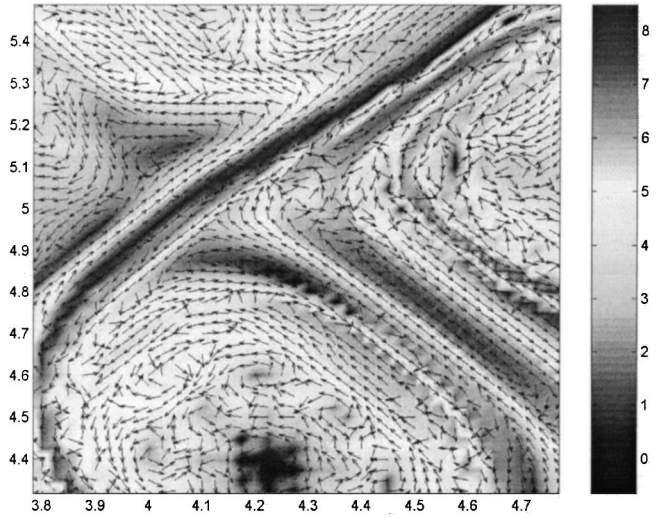

FIG. 4. The contours of $\sigma_t(\mathbf{x}_0)$, and the $\mathbf{e}_s(\mathbf{x}_0)$ vector field—as defined in (14)—for a two-dimensional barotropic turbulence simulation. [See Haller and Yuan (Ref. 3) for details.]

We now repeat the above construction in backward time for a unit vector $\mathbf{e}_u$, a candidate for a tangent to the $t=t_0$ slice of an attracting material line that contains $\overline{\mathbf{x}}(t)$. Again, a simple choice for $\mathbf{e}_u$ is

$$\mathbf{e}_u(\mathbf{x}_0)=\frac{(\nabla\mathbf{F}^{t_1})^{-1}\nabla\sigma_{t_0}(\overline{\mathbf{x}}(t_1))^\perp}{|(\nabla\mathbf{F}^{t_1})^{-1}\nabla\sigma_{t_0}(\overline{\mathbf{x}}(t_1))^\perp|},\tag{15}$$

where $\sigma_{t_0}(\overline{\mathbf{x}}(t_1))$ is based at positions at time t_1 and is computed in backward time up to time t_0. In the formula above, the tangent vector $\nabla\sigma_{t_0}(\overline{\mathbf{x}}(t_1))^\perp$ for the level curve of $\sigma_{t_0}(\overline{\mathbf{x}}(t_1))$ through $\overline{\mathbf{x}}(t_1)$ is mapped back to the initial configuration at $t=t_0$ by the inverse of the linearized flow map. In other words, $\mathbf{e}_u(\mathbf{x}_0)$, as defined above, is the inverse image of an approximate tangent vector to the candidate attracting material line at $t=t_1$. Again, other choices for $\mathbf{e}_u(\mathbf{x}_0)$ are possible. For instance, if velocity data is also available over the time interval $[t_{-1},t_0]$ for some $t_{-1}<t_0$, then a choice analogous to (14) gives $\mathbf{e}_u(\mathbf{x}_0)=\nabla\sigma_{-t_1}(\mathbf{x}_0)^\perp/|\nabla\sigma_{-t_1}(\mathbf{x}_0)^\perp|$.

We now define quantities whose role turns out to be similar to that of the quantities featured in the previous section. To emphasize this analogy, we use the same notation for these quantities, even though their actual definition will be different in our current context.

For any fixed initial position $\mathbf{x}_0$, we introduce the normalized Lagrangian strain rates

$$\begin{aligned}\lambda_1(t)&=-\frac{\langle\mathbf{e}_s,\nabla\mathbf{F}^t{}^*\mathbf{S}\nabla\mathbf{F}^t\mathbf{e}_s\rangle}{\langle\mathbf{e}_s,\nabla\mathbf{F}^t{}^*\nabla\mathbf{F}^t\mathbf{e}_s\rangle},\\ \lambda_2(t)&=\frac{\langle\mathbf{e}_u,\nabla\mathbf{F}^t{}^*\mathbf{S}\nabla\mathbf{F}^t\mathbf{e}_u\rangle}{\langle\mathbf{e}_u,\nabla\mathbf{F}^t{}^*\nabla\mathbf{F}^t\mathbf{e}_u\rangle},\end{aligned}\tag{16}$$

where $\mathbf{S}$ refers to $\mathbf{S}(\overline{\mathbf{x}}(t),t)=\frac{1}{2}[\nabla\mathbf{u}(\overline{\mathbf{x}}(t),t)+\nabla\mathbf{u}(\overline{\mathbf{x}}(t),t)^*]$, the rate-of-strain tensor evaluated along the trajectory $\overline{\mathbf{x}}(t)$ at time t. We again assume that

$$-\lambda_1(t)<0<\lambda_2(t), \tag{17}$$

holds over the time interval $I=[t_0,t_1]$, and define

$$\lambda_{k\min}=\min_{t\in I}\lambda_k(t), \quad k=1,2, \quad \lambda_{\min}=\min(\lambda_{1\min},\lambda_{2\min}).$$

We stress that (17) requires the two Lagrangian strains $\lambda_i(t)$ to keep their signs all over the interval I.

Next we define

$$\alpha=\min_{t\in I}\frac{|\det[\nabla\mathbf{F}^t\mathbf{e}_s,\nabla\mathbf{F}^t\mathbf{e}_u]|}{|\nabla\mathbf{F}^t\mathbf{e}_s||\nabla\mathbf{F}^t\mathbf{e}_u|}, \tag{18}$$

a constant that measures the minimal separation between advected counterparts of the initial vectors $\mathbf{e}_s$ and $\mathbf{e}_u$. We also re-introduce the following measures of modeling error from the previous section:

$$B_w=\max_{t\in I}\int_{t_0}^{t_1}B(\tau)w_t(\tau)\,d\tau, \quad L_w=\max_{t\in I}\int_{t_0}^{t_1}L(\tau)w_t(\tau)\,d\tau.$$

Finally, we redefine the distance Δ form the previous section as

$$\Delta=\begin{cases}\dfrac{\alpha\lambda_{\min}}{2\sqrt{2}C} & \text{if} \quad C>0\\[2ex] \dfrac{2}{\alpha} & \text{if} \quad C=0\end{cases}. \tag{19}$$

We are now ready to state a result analogous to Theorem 1.

Theorem 2: *Suppose that along a trajectory* $\overline{\mathbf{x}}(t)$ *of the model velocity field* $\mathbf{u}$, *condition* (17) *is satisfied. Assume further that*

$$B_wC<\frac{\alpha^2\lambda_{\min}}{8} \tag{20}$$

and

$$L_w<\frac{\alpha}{2\sqrt{2}}. \tag{21}$$

Then

(i) *the model trajectory* $\overline{\mathbf{x}}(t)$ *is contained in a hyperbolic material line* $\mathcal{M}(t)$ *over the time interval* I;

(ii) *the true velocity field* $\mathbf{v}(\mathbf{x},t)$ *admits a hyperbolic material line* $\mathcal{N}(t)$ *at least* Δ*-close to* $\mathcal{M}(t)$.

We prove this theorem in Appendix B. In the special case of zero modeling error ($B_w=L_w=0$), statement (i) of the theorem gives $\Delta=0$—which means that a hyperbolic material line passes through the point $\mathbf{x}_0$. This observation implies the following result.

Theorem 3: *A local extremum curve* l *of the scalar field* σ_t *corresponds to a repelling material line* $\mathcal{M}(t)$ (*with* $\mathcal{M}(t_0)=l$) *if*

$$\langle\mathbf{e}_s,\nabla\mathbf{F}^{t*}\mathbf{S}\nabla\mathbf{F}^t\mathbf{e}_s\rangle<0, \quad \langle\mathbf{e}_u,\nabla\mathbf{F}^{t*}\mathbf{S}\nabla\mathbf{F}^t\mathbf{e}_u\rangle>0 \tag{22}$$

hold for all $t\in I$ *along* l.

The sufficiency of condition (22) in the above statement follows from Theorem 2 after setting $B_w=L_w=0$.

Two remarks are in order. First, an inspection of the proof of Theorem 2 shows that if $\mathbf{e}_s$ is not just an approximate but an *exact* tangent vector to the candidate material line $\mathcal{M}(t)$, then conditions (22) become necessary for $\mathcal{M}(t)$ to be a repelling material line. [This is because the linear instability of $\mathcal{M}(t)$ necessarily implies (22), as seen from (B2).]

Second, the proof of Theorem 2 does not depend on the particular choice of the vectors $\mathbf{e}_s$ and $\mathbf{e}_u$. As we noted earlier, (14) and (15) are plausible choices, but other candidates can also be used. As long as these candidates satisfy (22), the repelling nature of $\mathcal{M}(t)$ follows.

V. IMPLICATIONS FOR OTHER LAGRANGIAN DIAGNOSTIC TOOLS

Theorem 3 can validate predictions by any Lagrangian method for locating hyperbolic coherent structures from flow data. Specifically, maximum curves of finite-time Lyapunov exponents,[15–17] finite-size Lyapunov exponents,[12] relative dispersion,[6,10,18,19] or entropy,[19] as well as lines of discontinuity of absolute dispersion or patchiness[20] all indicate finite-time hyperbolic material lines as long as the Lagrangian strain conditions (22) hold along them. Verifying these strain conditions requires the identification of the vectors $\mathbf{e}_0^s$ and $\mathbf{e}_0^u$, and the estimation of the modeling error.

VI. EXAMPLES

In this section, we give examples where our theorems can be evaluated analytically. The purpose of these examples is to give the reader a feel for the qualitative meaning of the results; more complex numerical velocity models will be treated elsewhere.

Example 1: The simplest example for the application of Theorem 1 is given by the velocity field

$$\mathbf{v}(\mathbf{x},t)=\mathbf{A}(t)\mathbf{x}+\boldsymbol{\mu}(\mathbf{x},t),$$

where the coefficient matrix $\mathbf{A}(t)$ is of the form

$$\mathbf{A}(t)=\begin{pmatrix}-\lambda(t) & 0\\ 0 & \lambda(t)\end{pmatrix},$$

with some continuous function $\lambda(t)>0$. We assume the velocity error $\mu(\mathbf{x},t)$ to be Lipschitz in $\mathbf{x}$ with Lipschitz constant $L(t)$ for any fixed $t\in I$ [see (3)]. We also assume that $|\mu(\mathbf{x},t)|<B(t)$ for $t\in I$.

Since $\mathbf{u}(\mathbf{x},t)$ is linear, we have $C=0$ [see (2)]. Furthermore, the eigenvectors of $\mathbf{A}(t)$ are constant and orthogonal, thus (7) gives $\alpha=1$, $\beta=0$. We also see that for any finite time interval I,

$$\lambda_{\min}=\min_{t\in I}\lambda(t).$$

Then Theorem 1 guarantees the existence of a repelling material line $\mathcal{N}(t)$ near $\mathbf{x}=0$, provided that

$$\max_{t\in[t_0,t_1]}\int_{t_0}^{t_1}L(\tau)w_t(\tau)\,d\tau<\frac{1}{\sqrt{2}}.$$

Moreover, by Theorem 1, the distance of $\mathcal{N}(t)$ from the origin $\mathbf{x}=0$ is less than

$$\Delta = 2.$$

Notice that the magnitude of the modeling error is not constrained by the above results: Only the Lipschitz constant of the error must obey a bound. The reason for only a single condition is the linearity of $\mathbf{u}$, which causes C to vanish.

Since the model velocity field can be solved explicitly by exponentiating the matrix $\mathbf{A}(t)$, applying Theorem 2 to the above example will lead to the same result.

Example 2: To illustrate the application of Theorem 2, we consider the velocity field

$$\mathbf{v}(\mathbf{x},t)=\mathbf{A}(t)\mathbf{x}+\mathbf{f}(\mathbf{x},t)+\boldsymbol{\mu}(\mathbf{x},t), \tag{23}$$

with

$$\mathbf{A}(t)=\begin{pmatrix} \sin 2\omega t & \omega+\cos 2\omega t \\ -\omega+\cos 2\omega t & -\sin 2\omega t \end{pmatrix}, \quad \mathbf{f}(\mathbf{x},t)=\begin{pmatrix} 0 \\ \frac{1}{3}x_1^3 \end{pmatrix}.$$

Again, we assume that $\mu(\mathbf{x},t)$ is Lipschitz in $\mathbf{x}$ over the box

$$U_{\delta_0}=\{\mathbf{x}\in\mathbb{R}^2 \,|\, |x_1|\leqslant\delta_0\},$$

with Lipschitz constant $L(t)$. We also require $\boldsymbol{\mu}(\mathbf{x},t)$ to be bounded in norm by $B(t)$. Note that within U_{δ_0}, we have the estimate

$$|\nabla^2\mathbf{u}(\mathbf{x},t)|\leqslant C\equiv 2\delta_0. \tag{24}$$

For $|\omega|>1$, the eigenvalues of $\nabla\mathbf{u}(\mathbf{0},t)=\mathbf{A}(t)$ are $\pm i\sqrt{\omega^2-1}$. This eigenvalue configuration does not satisfy the basic assumptions of Sec. III: the $\mathbf{x}=\mathbf{0}$ stagnation point is not Okubo–Weiss hyperbolic. Following the approach of Sec. IV instead, one finds that $\nabla\mathbf{F}^t(\mathbf{0})$ can be calculated explicitly:

$$\nabla\mathbf{F}^t(\mathbf{0})=\begin{pmatrix} \cos\omega t & -\sin\omega t \\ \sin\omega t & \cos\omega t \end{pmatrix}\begin{pmatrix} e^{-t} & 0 \\ 0 & e^{t} \end{pmatrix}. \tag{25}$$

This formula shows that the origin is finite-time hyperbolic over any time interval I. For $\boldsymbol{\mu}\equiv\mathbf{0}$, classic invariant manifold theorems guarantee that $\mathbf{x}=\mathbf{0}$ admits stable and unstable manifold in the extended phase space. These manifolds are tangent to the stable and unstable bundles of $\nabla\mathbf{F}^t(\mathbf{0})$; the asymptotic decay rates of solutions in them are given by $e^{\mp t}$ in forward and backward time, respectively.

Based on the above, the scalar field $\underline{\sigma}_t(\mathbf{x}_0)$ will admit a local maximizing curve that contains the $\overline{\mathbf{x}}=\mathbf{0}$ solution of the model velocity field. This curve is the DLE approximation of the $t=t_0$ slice of the local stable manifold of the origin. For large enough t, the maximizing curve becomes close enough to the actual stable manifold, and hence the vector $\mathbf{e}_s(\mathbf{0})$ defined in (14) becomes a good approximation for the tangent of the manifold at the origin. In that case, (16) gives $\lambda_1(t)=1$. Similarly, a backward-time DLE calculation yields $\lambda_2(t)=1$, which then gives

$$\lambda_{\min}=1.$$

Furthermore, as seen from (25), the two vectors $\mathbf{e}_s(\mathbf{0})$ and $\mathbf{e}_u(\mathbf{0})$ are orthogonal, leading to the α value [see (18)]

$$\alpha=1.$$

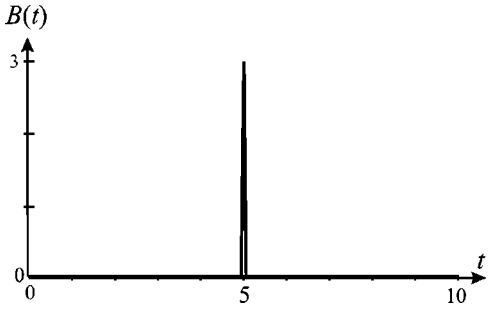

FIG. 5. Spiky velocity error over the time interval $I=[0,10]$. The magnitude of the error increases linearly from zero to one over the interval $[4.95,5]$, and decreases back to zero linearly over the interval $[5,5.05]$.

These observations give the following form of condition (20) in this example:

$$B_w=\max_{t\in I}\int_{t_0}^{t_1}B(\tau)w_t(\tau)\,d\tau\leqslant\frac{1}{16\delta_0}, \tag{26}$$

imposing the upper bound

$$\delta_0\leqslant\frac{1}{16B_w} \tag{27}$$

on the size of the U_{δ_0} ball in our analysis. At the same time, an inspection of the proof of Theorem 1 shows that hyperbolic material lines can be constructed in the U_Δ box around the origin, with Δ defined in (19). This observation implies that we must have $\Delta=1/(4\sqrt{2}\delta_0)<\delta_0$, or equivalently, $\delta_0>1/(2\sqrt[4]{2})$, which together with (27) gives the condition

$$B_w<\frac{\sqrt[4]{2}}{8}\approx 0.1487. \tag{28}$$

As for condition (21) of Theorem 1, we obtain

$$L_w=\max_{t\in I}\int_{t_0}^{t_1}L(\tau)w_t(\tau)\,d\tau\leqslant\frac{1}{2\sqrt{2}}\approx 0.3536. \tag{29}$$

We conclude that if (28) and (29) are satisfied, then Theorem 2 gives the existence of attracting and repelling material lines within the U_Δ ball for the true velocity field (23) with

$$\Delta=\frac{1}{4\sqrt{2}\delta_0}<\frac{\sqrt[4]{2}}{2\sqrt{2}}\approx 0.4204. \tag{30}$$

As a simple example, let us fix the time interval $I=[0,10]$, and consider the spatially uniform velocity error $\boldsymbol{\mu}(t)=(0,\mu_2(t))$ with

$$\mu_2(t)=\begin{cases} 0 & \text{if} \quad 0\leqslant t\leqslant 4.95 \\ 3(t-4.95) & \text{if} \quad 4.95<t\leqslant 5 \\ -3(t-5.05) & \text{if} \quad 5<t\leqslant 5.05 \\ 0 & \text{if} \quad 5.05<t\leqslant 10 \end{cases}.$$

The magnitude of $|\boldsymbol{\mu}(t)|=B(t)$ is shown in Fig. 5. We find the time-weighted measures of the velocity error to be

$$B_w=0.1476, \quad L_w=0.$$

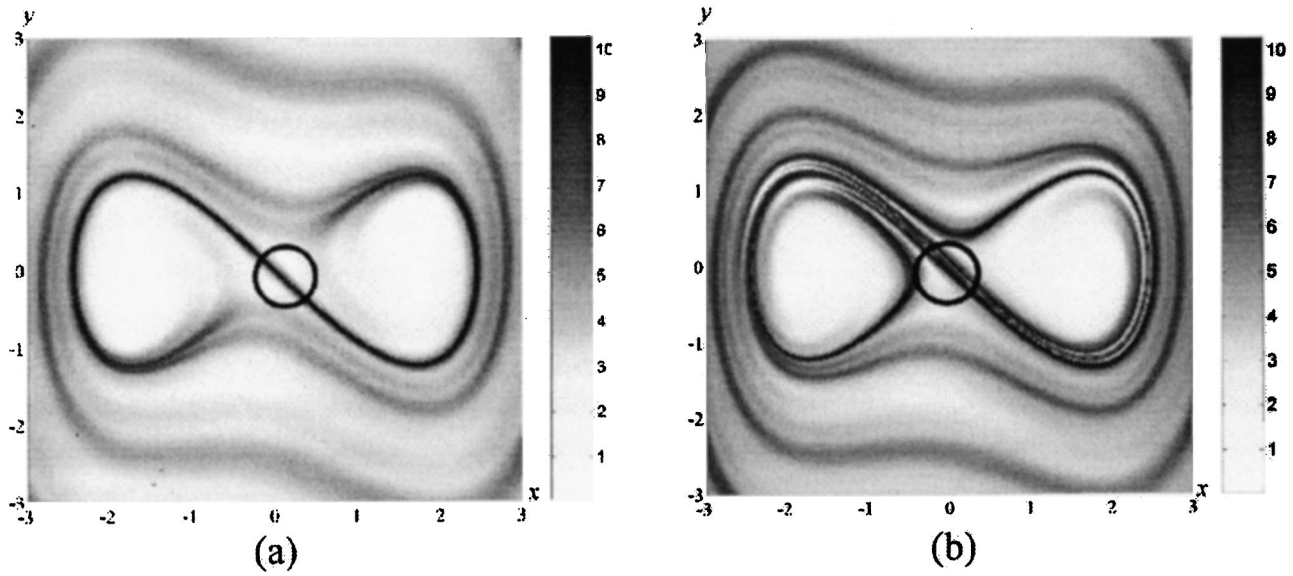

FIG. 6. The $\mathrm{DLE}_t(\mathbf{x}_0)$ field for Example 2, with $t_0=0$ and $t=10$. The circle indicates the location of the ball U_Δ. (a) Model velocity field; (b) true velocity field.

The first of these measures is obtained from numerical integration, while the second one is zero because the modeling error is independent of $\mathbf{x}$. These values satisfy the inequalities (28) and (29), thus a hyperbolic material line $\mathcal{N}(t)$ near the origin will survive in the true velocity field. We obtain from Theorem 1 and (30) that the distance of $\mathcal{N}(t)$ from the origin does not exceed $\Delta=0.4204$.

We show the results of a DLE calculation for the model and for the true velocity field in Fig. 6. Since our calculations have remained independent of the parameter ω, we selected $\omega=0$ in our simulation to minimize numerical errors. The figure shows that while the global stable manifold—an attracting material line—of the model velocity field deforms noticeably, it does survive the effect of the spiky error term, and remains close to its original position within the ball U_Δ.

Example 3: This example will show how Theorem 3 distinguishes spurious maximizing curves of Lyapunov exponents—arising from maximal shear—from hyperbolic material lines. Let us consider a parallel shear flow of the form

$$\mathbf{v}(\mathbf{x},t)=\begin{pmatrix} u(y) \\ 0 \end{pmatrix}, \quad \mathbf{x}=\begin{pmatrix} x \\ y \end{pmatrix}.$$

The trajectories satisfy

$$x(t)=x_0+u(y_0)\,(t-t_0), \quad y(t)=y_0, \tag{31}$$

from which we obtain

$$\nabla\mathbf{F}^t(\mathbf{x}_0)=\begin{pmatrix} 1 & u'(y_0)\,(t-t_0) \\ 0 & 1 \end{pmatrix}, \tag{32}$$

with prime denoting differentiation with respect to y_0. This formula shows that the Cauchy–Green strain σ_t only depends on the y_0 coordinate of an initial condition $\mathbf{x}_0=(x_0,y_0)$. An implicit differentiation of the characteristic equation of the matrix $[\nabla\mathbf{F}^t(\mathbf{x}_0)]^*\nabla\mathbf{F}^t(\mathbf{x}_0)$ further yields

$$\begin{aligned} \sigma_t' &= \frac{2u'u''(t-t_0)^2\sigma_t}{2\sigma_t+(u')^2(t-t_0)^2+2}, \\ \sigma_t'' &= \frac{2\sigma_t[(u'')^2+u'u''']-2(\sigma_t')^2}{2\sigma_t+(u')^2+2}. \end{aligned} \tag{33}$$

Assume now that u' is positive and locally maximal at $y_0=\eta$, i.e.,

$$u'(\eta)>0, \quad u''(\eta)=0, \quad u'''(\eta)<0.$$

We show the corresponding velocity profile in Fig. 7.

By (33), we have

$$\sigma_t'(\eta)=0, \quad \sigma_t''(\eta)=\frac{2\sigma_t(\eta)u'(\eta)u'''(\eta)}{2\sigma_t(\eta)+(u'(\eta))^2+2}<0,$$

which shows that the $y_0=\eta$ line is a local maximizing curve for $\sigma_t(y_0)$ and hence for the direct Lyapunov exponent field $\mathrm{DLE}_t(\mathbf{x}_0)$. Yet, as (31) shows, no hyperbolic material lines (stable or unstable manifolds) exist in this flow. Therefore, as we noted earlier, local maximizing curves of Lyapunov exponent plots do not imply local hyperbolicity in the flow; they may also be indicators of high shear.

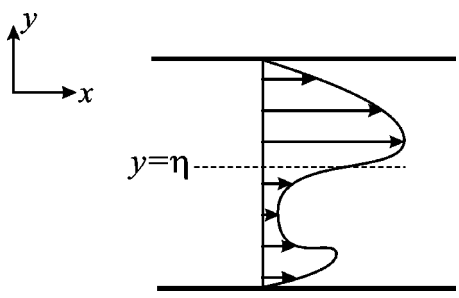

FIG. 7. Velocity profile for Example 3.

We now show how Theorem 3 reveals that the above maximizing curve of the Lyapunov exponent field is a nonhyperbolic material line. From (14), (32), and from the definition of the rate of strain we obtain

$$\mathbf{e}_s(\mathbf{x}_0)=\begin{pmatrix}1\\0\end{pmatrix},\quad \mathbf{S}=\frac{1}{2}\begin{pmatrix}0 & u'\\ u' & 0\end{pmatrix},$$

$$\nabla\mathbf{F}^t{}^*\mathbf{S}\nabla\mathbf{F}^t=\frac{1}{2}\begin{pmatrix}0 & u'\\ u' & 2(u')^2\end{pmatrix},$$

which leads to

$$\langle \mathbf{e}_s,\nabla\mathbf{F}^t{}^*\mathbf{S}\nabla\mathbf{F}^t\mathbf{e}_s\rangle\equiv 0$$

or $\lambda_1(t)\equiv 0$. Therefore, even though $y_0=\eta$ is a local maximizer of the finite-time Lyapunov exponent field $\mathrm{DLE}_t(\mathbf{x}_0)$, it is a nonhyperbolic material line by our first remark after Theorem 3.

VII. CONCLUSIONS

In this paper we have examined the relevance of Lagrangian coherent structures—finite-time stable and unstable manifolds extracted from model velocity data—for the true flow. We have found that Lagrangian coherent structures are surprisingly robust: even large velocity errors will preserve them as long as those errors are small in a special time-weighted norm. The weight function in this norm turns out to decay exponentially in time, allowing for temporally localized spikes in both the error and its gradient.

In more mathematical terms, Theorems 1 and 2 give conditions under which the modeling error can be viewed as a small perturbation to the flow map, the map that takes initial particle positions at $t=t_0$ to later positions at $t=t_1$. In this sense, this paper provides a quantitative relation between deterministic Eulerian errors and their effect on the finite-time Lagrangian flow.

We summarized our main qualitative results in the Introduction. We have also shown the quantitative use of our criteria through simple examples in Sec. VI. An application of these criteria to surface velocity measurements in Monterey Bay will appear elsewhere.

A much-needed extension of our analysis would incorporate stochastic terms in the velocity error. Preliminary work in this direction indicates a similar robustness of Lagrangian coherent structures for stochastic noise, although under somewhat different conditions.

A further extension of interest will be the treatment of three-dimensional (3D) flows. Such an extension appears plausible based on the available 3D extensions for the Lagrangian Okubo–Weiss criterion and for the direct Lyapunov exponent algorithm.[7]

ACKNOWLEDGMENTS

This research was partially supported by AFOSR Grant No. F49620-00-1-0133, NSF Grant No. DMS-98-00922, and a United Technologies research grant. The author would like to thank Bernard Legras and the anonymous referee for their close and critical reading of the manuscript, as well as for their valuable suggestions.

APPENDIX A: PROOF OF THEOREM 1

1. Setup

As in Ref. 2, we start by introducing the change of coordinates $\mathbf{y}=\mathbf{x}-\overline{\mathbf{x}}(t)$, which puts (1) in the form

$$\dot{\mathbf{y}}=\nabla\mathbf{u}(\overline{\mathbf{x}}(t),t)\mathbf{y}+\boldsymbol{\mu}(\overline{\mathbf{x}}(t)+\mathbf{y},t)+\mathcal{O}(|\mathbf{y}|^2), \tag{A1}$$

where the $\mathcal{O}(|y|^2)$ terms also depend on t. We recall that the matrix $\mathbf{T}(t)$ contains the normalized real eigenvectors of $\nabla\mathbf{u}(\overline{\mathbf{x}}(t),t)$ that exist under assumption (4). We pass to eigenbasis along $\overline{\mathbf{x}}(t)$ by letting $\mathbf{y}=\mathbf{T}(t)\mathbf{z}$, which yields the transformed system

$$\dot{\mathbf{z}}=\boldsymbol{\Lambda}(t)\mathbf{z}+\mathbf{R}(\mathbf{z},t)+\mathbf{P}(\mathbf{z},t)-\mathbf{Q}(\mathbf{z},t), \tag{A2}$$

with

$$\boldsymbol{\Lambda}(t)=\mathrm{diag}\ \ (-\lambda_1(t),\lambda_2(t)),$$

$$\mathbf{R}(\mathbf{z},t)=\mathbf{T}^{-1}(t)\boldsymbol{\mu}(\overline{\mathbf{x}}(t)+\mathbf{T}(t)\mathbf{z},t)$$

and

$$\mathbf{P}(\mathbf{z},t)=\mathcal{O}(\|\mathbf{T}^{-1}\|\|\mathbf{T}\mathbf{z}|^2),\quad \mathbf{Q}(\mathbf{z},t)=\mathbf{T}^{-1}\dot{\mathbf{T}}\mathbf{z}.$$

From the definitions of α, β, C, and $B(t)$, we obtain

$$|\mathbf{P}(\mathbf{z},t)|\leqslant\frac{\sqrt{2}C}{2\alpha}|\mathbf{z}|^2,\quad |\mathbf{Q}(\mathbf{z},t)|\leqslant\frac{\sqrt{2}\beta}{\alpha}|\mathbf{z}|.$$

$$|\mathbf{R}(\mathbf{z},t)|\leqslant\frac{\sqrt{2}}{\alpha}B(t),\quad |\mathbf{R}(\mathbf{z},t)-\mathbf{R}(\tilde{\mathbf{z}},t)|\leqslant\frac{\sqrt{2}}{\alpha}L(t)|\mathbf{z}-\tilde{\mathbf{z}}|.$$

2. Integral equations

As in Ref. 2, we fix two small constants $\delta,d>0$ and modify (A2) in a C^∞ fashion so that the modified vector field

$$\dot{\mathbf{z}}=\overline{\boldsymbol{\Lambda}}(t)\mathbf{z}+\overline{\mathbf{R}}(\mathbf{z},t)+\overline{\mathbf{P}}(\mathbf{z},t)-\overline{\mathbf{Q}}(\mathbf{z},t), \tag{A3}$$

becomes Lipschitz for all $\mathbf{z}\in\mathbb{R}^2$ and $t\in\mathbb{R}$, coincides with Eq. (A2) for $|\mathbf{z}|\leqslant\delta$ and $t\in[t_0+d,t_1-d]$, and obeys the estimates

$$\tilde{\Lambda}_{11}(t)\leqslant-\lambda_{1\min}<0<\lambda_{2\min}\leqslant\tilde{\Lambda}_{22}(t),$$

$$\tilde{\Lambda}_{12}(t)=\tilde{\Lambda}_{21}(t)\equiv 0,\quad t\in\mathbb{R},$$

$$|\overline{\mathbf{P}}(\mathbf{z},t)|\leqslant\delta\frac{\sqrt{2}C}{2\alpha}|\mathbf{z}|,\quad |\overline{\mathbf{Q}}(\mathbf{z},t)|\leqslant\frac{\sqrt{2}\beta}{\alpha}|\mathbf{z}|,$$

$$|\overline{\mathbf{R}}(\mathbf{z},t)|\leqslant\frac{\sqrt{2}}{\alpha}B(t),\quad |\overline{\mathbf{R}}(\mathbf{z},t)-\overline{\mathbf{R}}(\overline{\mathbf{z}},t)|\leqslant\frac{\sqrt{2}}{\alpha}L(t)|\mathbf{z}-\overline{\mathbf{z}}|,$$

$$\overline{\mathbf{P}}(\mathbf{z},t)=\overline{\mathbf{Q}}(\mathbf{z},t)\equiv\mathbf{0}\quad\text{and}\quad B(t)=L(t)\equiv 0$$
$$\text{for}\ \ t\notin[t_0,t_1]\quad\text{or}\quad |\mathbf{z}|>2\delta. \tag{A4}$$

For more details of this construction see Ref. 2 or 7.

We introduce the notation

$$\mathbf{z}=(z_s,z_u),\qquad \overline{\mathbf{P}}=(\tilde{P}_s,\tilde{P}_u),\quad \overline{\mathbf{Q}}=(\tilde{Q}_s,\tilde{Q}_u),$$

$$\overline{\mathbf{R}}=(\tilde{R}_s,\tilde{R}_u),\quad \tilde{\lambda}_1=\tilde{\Lambda}_{11},\quad \tilde{\lambda}_2=\tilde{\Lambda}_{22},$$

then drop the tildes and integrate (A3) to obtain

$$z_s(t)=e^{-\int_{t_s}^{t}\lambda_1(\tau)d\tau}z_s(t_s)+\int_{t_s}^{t}e^{-\int_{\tau}^{t}\lambda_1(s)ds}\times[P_s(\mathbf{z}(\tau),\tau)+Q_s(\mathbf{z}(\tau),\tau)+R_s(\mathbf{z}(\tau),\tau)]d\tau,$$
$$z_u(t)=e^{\int_{t_u}^{t}\lambda_2(\tau)d\tau}z_u(t_u)+\int_{t_u}^{t}e^{\int_{\tau}^{t}\lambda_2(s)ds}\times[P_u(\mathbf{z}(\tau),\tau)+Q_u(\mathbf{z}(\tau),\tau)+R_u(\mathbf{z}(\tau),\tau)]d\tau. \tag{A5}$$

We want to construct an invariant set $\mathcal{N}$ that contains bounded solutions to the above integral equation. If nonempty, $\mathcal{N}$ will be an exceptional invariant set because most solutions near $\mathbf{z}=\mathbf{0}$ grow due to the positive exponent in the second equation of (A5). Once a solution leaves the 2δ-ball outside which the velocity field is linear, it will further grow without bound. As we shall see, the subset of $\mathcal{N}$ falling in the interval $t\in[t_0+d,t_1-d]$ serves as a finite-time stable set for a trajectory that is close to the original solution $\overline{\mathbf{x}}(t)$ of the model velocity field.

For any fixed initial time t_0, we first define $\mathcal{N}(t_0)$ as

$$\mathcal{N}(t_0)=\{\mathbf{z}_0|\sup_{t\geqslant t_0}|\mathbf{z}(t;\mathbf{z}_0)|<\infty\}, \tag{A6}$$

where $\mathbf{z}(t_0;\mathbf{z}_0)=\mathbf{z}_0$. Note that $\mathcal{N}(t_0)$ is a positively invariant family of sets indexed by t_0. Furthermore, for any fixed $t\in\mathbb{R}$ and for any potential solution $\mathbf{z}(t)\in\mathcal{N}(t)$, we have

$$\lim_{t_u\to\infty}|e^{\int_{t_u}^{t}\lambda_2(\tau)\ d\tau}z_u(t_u)|\leqslant K\lim_{t_u\to\infty}e^{\int_{t_u}^{t}\lambda_2(\tau)\ d\tau}=0.$$

As a result, taking the limit $t_u\to\infty$ in (A5), setting $t_s=t_0$ and $z_s(t_s)=z_s$, we obtain the following integral equation for solutions in $\{(\mathcal{N}(t),t)\mid t\in\mathbb{R}\}$:

$$z_s(t)=e^{-\int_{t_0}^{t}\lambda_1(\tau)d\tau}z_s+\int_{t_0}^{t}e^{-\int_{\tau}^{t}\lambda_1(s)ds}\times[P_s(\mathbf{z}(\tau),\tau)+Q_s(\mathbf{z}(\tau),\tau)+R_s(\mathbf{z}(\tau),\tau)]d\tau,$$
$$z_u(t)=\int_{\infty}^{t}e^{\int_{\tau}^{t}\lambda_2(s)\ ds}[P_u(\mathbf{z}(\tau),\tau)+Q_u(\mathbf{z}(\tau),\tau)+R_u(\mathbf{z}(\tau),\tau)]d\tau. \tag{A7}$$

We shall prove that for any small enough z_s, this integral equation has a unique solution $\mathbf{z}(t)$ with $z_s(0)=z_s$.

3. Finite-time hyperbolicity

Equation (A7) can be rewritten as a functional equation of the form

$$\mathbf{z}(t)=\mathcal{F}(\mathbf{z}(t)), \tag{A8}$$

which shows that any solution contained in $\mathcal{N}(t)$ is a fixed point of $\mathcal{F}$. Using the norm

$$\|\mathbf{z}\|=\sup_{t\geqslant 0}|\mathbf{z}(t)|, \tag{A9}$$

we shall view $\mathcal{F}$ as a map on the function space

$$B=\{\boldsymbol{\phi}=(\phi_s,\phi_u):[0,\infty)\to\mathbb{R}^2|\ \boldsymbol{\phi}\in C^0[0,\infty),\ \|\boldsymbol{\phi}\|\leqslant\delta,\quad \phi_s(t_0)=\delta^*\},$$

where $0<\delta^*<\delta$ are positive constants to be determined later. Note that B is a complete metric space in the norm $\|\cdot\|$. We want to show that $\mathcal{F}$ is a contraction mapping on B, which in turn will imply the existence of a unique solution to (A8). This solution will automatically be a solution of the unmodified differential equation (A2) by the definition of the space B.

First, we want to show that $\mathcal{F}$ maps the space B into B. From the integral equation (A7) and the estimates (A4) we obtain

$$|\mathcal{F}_s(\mathbf{z}(t))|\leqslant e^{-\int_{t_0}^{t}\lambda_1(\tau)\ d\tau}|z_s|+\int_{t_0}^{t}e^{-\int_{\tau}^{t}\lambda_1(s)\ ds}[|P_s(\mathbf{z}(\tau),\tau)|+|Q_s(\mathbf{z}(\tau),\tau)|+|R_s(\mathbf{z}(\tau),\tau)|]\,d\tau,$$
$$|\mathcal{F}_u(\mathbf{z}(t))|\leqslant\int_{t}^{\infty}e^{\int_{\tau}^{t}\lambda_2(s)\ ds}[|P_u(\mathbf{z}(\tau),\tau)|+|Q_u(\mathbf{z}(\tau),\tau)|+|R_u(\mathbf{z}(\tau),\tau)|]\ d\tau, \tag{A10}$$

which leads to

$$|\mathcal{F}_s(\mathbf{z}(t))|\leqslant\delta^*e^{-\int_{t_0}^{t}\lambda_1(\tau)\ d\tau}+\left[\delta\frac{\sqrt{2}C}{2\alpha}+\frac{\sqrt{2}\beta}{\alpha}\right]\int_{t_0}^{t}e^{-\int_{\tau}^{t}\lambda_1(s)\ ds}|\mathbf{z}|\,d\tau+\frac{\sqrt{2}}{\alpha}\int_{t_0}^{t}e^{-\int_{\tau}^{t}\lambda_1(s)\ ds}B(\tau)\ d\tau,$$
$$|\mathcal{F}_u(\mathbf{z}(t))|\leqslant\left[\delta\frac{\sqrt{2}C}{2\alpha}+\frac{\sqrt{2}\beta}{\alpha}\right]\int_{t}^{t_1}e^{\int_{\tau}^{t}\lambda_2(s)\ ds}|\mathbf{z}|\,d\tau+\frac{\sqrt{2}}{\alpha}\int_{t}^{t_1}e^{\int_{\tau}^{t}\lambda_2(s)\ ds}B(\tau)\,d\tau. \tag{A11}$$

Here the integrands on the right-hand side of the inequalities are to be replaced with zero for t values outside the interval $[t_0,t_1]$, since the integrands in (A10) vanish outside $[t_0,t_1]$. We now add the last two inequalities and take the suprema of both sides over $t\geqslant 0$. (On the right-hand side of the summed inequality, this will simply amount to taking the maximum over the compact interval $[t_0,t_1]$.) Then, recalling the definition of the norm $\|\cdot\|$ from (A9), we obtain that

$$\|\mathcal{F}(\mathbf{z}(t))\|\leqslant\max_{t\in I}[|\mathcal{F}_s(\mathbf{z}(t))|+|\mathcal{F}_u(\mathbf{z}(t))|]\leqslant\delta,$$

holds if

$$\delta^*+\left[\delta\frac{\sqrt{2}C}{2\alpha}+\frac{\sqrt{2}\beta}{\alpha}\right]\left[\frac{1}{\lambda_{1\,\min}}+\frac{1}{\lambda_{2\,\min}}\right]\delta+\frac{\sqrt{2}}{\alpha}B_w\leqslant\delta, \tag{A12}$$

is satisfied. This inequality will hold for appropriate $\delta^*>0$ if we require

$$\left[\delta\frac{\sqrt{2}C}{2\alpha}+\frac{\sqrt{2}\beta}{\alpha}\right]\frac{2\delta}{\lambda_{\min}}+\frac{\sqrt{2}}{\alpha}B_w<\delta. \tag{A13}$$

In summary, under condition (A13), there exists small $\delta^*>0$, such that $\mathcal{F}$ maps the function space B into itself.

Next we want to find a condition for $\mathcal{F}$ to be a contraction mapping on the space B. This is the case if there exists a positive constant $q<1$, such that for any two functions $\mathbf{z}(t),\hat{\mathbf{z}}(t)\in B$, we have $\|\mathcal{F}(\mathbf{z}(t))-\mathcal{F}(\hat{\mathbf{z}}(t))\|\leqslant q\|\mathbf{z}(t)-\hat{\mathbf{z}}(t)\|$. Estimates similar to (A11)–(A13) lead to

$$\|\mathcal{F}(\mathbf{z}(t))-\mathcal{F}(\hat{\mathbf{z}}(t))\| \leqslant\left[\left(\delta\frac{\sqrt{2}C}{2\alpha}+\frac{\sqrt{2}\beta}{\alpha}\right)\frac{2}{\lambda_{\min}}+\frac{\sqrt{2}}{\alpha}L_w\right]\|\mathbf{z}(t)-\hat{\mathbf{z}}(t)\|. \quad \text{(A14)}$$

This inequality shows that $\mathcal{F}$ is a contraction mapping on the space B if

$$\left(\delta\frac{\sqrt{2}C}{2\alpha}+\frac{\sqrt{2}\beta}{\alpha}\right)\frac{2}{\lambda_{\min}}+\frac{\sqrt{2}}{\alpha}L_w<1. \quad \text{(A15)}$$

We have therefore obtained that under conditions (A13) and (A15), the map $\mathcal{F}$ is a contraction on the space B for small enough $\delta^*>0$. As a result, $\mathcal{F}$ admits a unique fixed point for small enough δ^*. This means that the set

$$\mathcal{N}=\{(\mathcal{N}(t),t)\mid t\in[t_0,t_1]\}, \quad \text{(A16)}$$

is not empty [see (A6)].

4. Lipschitz continuity

From the second equation of (A7), we obtain that

$$\begin{aligned}|z_u(t)-\hat{z}_u(t)|&\leqslant\left[\left(\delta\frac{\sqrt{2}C}{2\alpha}+\frac{\sqrt{2}\beta}{\alpha}\right)\frac{1}{\lambda_{2\min}}+\frac{\sqrt{2}L_w}{\alpha}\right]\\&\quad\times|\mathbf{z}(t)-\hat{\mathbf{z}}(t)|\\&\leqslant\left[\left(\delta\frac{\sqrt{2}C}{2\alpha}+\frac{\sqrt{2}\beta}{\alpha}\right)\frac{1}{\lambda_{2\min}}+\frac{\sqrt{2}L_w}{\alpha}\right]\\&\quad\times(|z_u(t)-\hat{z}_u(t)|+|z_s(t)-\hat{z}_s(t)|),\end{aligned}$$

which in turn gives

$$|z_u(t)-\hat{z}_u(t)|\leqslant\frac{|z_s(t)-\hat{z}_s(t)|}{\left[1-\left(\delta\frac{\sqrt{2}C}{2\alpha}+\frac{\sqrt{2}\beta}{\alpha}\right)\frac{1}{\lambda_{2\min}}+\frac{\sqrt{2}L_w}{\alpha}\right]}, \quad \text{(A17)}$$

provided that

$$\left[\delta\frac{\sqrt{2}C}{2\alpha}+\frac{\sqrt{2}\beta}{\alpha}\right]\frac{1}{\lambda_{2\,\min}}+\frac{\sqrt{2}L_w}{\alpha}<1.$$

But this last inequality will certainly hold whenever (A15) holds. As a result, $\mathcal{N}(t)$ is a Lipschitz graph over z_s by the estimate (A17).

5. Final set of conditions

To complete the proof, we need to find a set of conditions under which (A13) and (A15) both hold.

First, we assume that $C\neq0$ and note that the inequality (A13) holds for $\delta_-<\delta<\delta_+$, where

$$\delta_\pm=\frac{\alpha\lambda_{\min}-2\sqrt{2}\beta}{2\sqrt{2}C}\pm\sqrt{\frac{(\alpha\lambda_{\min}-2\sqrt{2}\beta)^2}{8C^2}-\frac{\lambda_{\min}B_w}{C}}.$$

For this condition to be meaningful, we must have $\delta_+>0$ ($\delta>0$ must hold), which holds if

$$B_wC<\frac{(\alpha\lambda_{\min}-2\sqrt{2}\beta)^2}{8\lambda_{\min}},\quad \lambda_{\min}>2\sqrt{2}\,\frac{\beta}{\alpha}. \quad \text{(A18)}$$

At this point, we can choose any $\delta\in(\delta_+,\delta_-)$ in our estimates. Computationally the simplest is the choice

$$\delta=\Delta\overset{\text{def.}}{=}\frac{\alpha\lambda_{\min}-2\sqrt{2}\beta}{2\sqrt{2}C}. \quad \text{(A19)}$$

The second basic condition (A15) is equivalent to

$$L_w<\frac{\alpha\lambda_{\min}-2\sqrt{2}\beta-\sqrt{2}C\delta}{\sqrt{2}\lambda_{\min}}.$$

With the δ value we selected in (A19), this last inequality becomes

$$L_w<\frac{\alpha\lambda_{\min}-2\sqrt{2}\beta-\sqrt{2}C\Delta}{\sqrt{2}\lambda_{\min}}=\frac{\alpha\lambda_{\min}-2\sqrt{2}\beta}{2\sqrt{2}\lambda_{\min}}. \quad \text{(A20)}$$

But (A18) and (A20) are precisely the assumptions of Theorem 1.

Assume now that $C=0$. Then (A13) gives

$$B_w<\delta\frac{\alpha\lambda_{\min}-2\sqrt{2}\beta}{\sqrt{2}\lambda_{\min}},$$

from which we obtain the condition

$$\delta>\frac{\sqrt{2}\lambda_{\min}}{\alpha\lambda_{\min}-2\sqrt{2}\beta}.$$

Therefore, any large enough δ can be selected for fixed B_w. We pick a δ that satisfies

$$\frac{\sqrt{2}\lambda_{\min}}{\alpha\lambda_{\min}-2\sqrt{2}\beta}<\delta=\Delta\overset{\text{def.}}{=}\frac{2\lambda_{\min}}{\alpha\lambda_{\min}-2\sqrt{2}\beta}. \quad \text{(A21)}$$

The second basic condition (A15) now gives

$$L_w<\frac{\alpha\lambda_{\min}-2\sqrt{2}\beta}{\sqrt{2}\lambda_{\min}},$$

which certainly holds if

$$L_w<\frac{\alpha\lambda_{\min}-2\sqrt{2}\beta}{2\sqrt{2}\lambda_{\min}}. \quad \text{(A22)}$$

Again, (A21) and (A22) complete the proof of (i) of Theorem 1 for $C=0$.

Once conditions (A18) and (A20) [or, for $C=0$, (A21) and (A22)] are satisfied for some $B_w,L_w>0$, then they are automatically satisfied for $B_w=L_w=0$. This implies the existence of the material line $\mathcal{M}(t)$ described in statement (i) of the theorem. Both $\mathcal{M}(t)$ and $\mathcal{N}(t)$ are known to exist in a δ-ball around the trajectory $\overline{\mathbf{x}}(t)$. The upper bound on δ in

our construction has been Δ, therefore, $\mathcal{N}(t)$ and $\mathcal{M}(t)$ are locally at least Δ-close to each other, as stated in (ii) of Theorem 1.

APPENDIX B: PROOF OF THEOREM 2

The proof of Theorem 2 follows the approach taken in the proof of Theorem 1. We again start by changing coordinates via $\mathbf{y}=\mathbf{x}-\overline{\mathbf{x}}(t)$, which yields the localized equation

$$\dot{\mathbf{y}}=\nabla\mathbf{u}(\overline{\mathbf{x}}(t),t)\mathbf{y}+\boldsymbol{\mu}(\overline{\mathbf{x}}(t)+\mathbf{y},t)+\mathcal{O}(|\mathbf{y}|^2).$$

This time, however, our second change of coordinates $\mathbf{y}=\mathbf{T}(t)\mathbf{z}$ is defined through the matrix

$$\mathbf{T}(t)=\left[\frac{\nabla\mathbf{F}^t\mathbf{e}_s}{|\nabla\mathbf{F}^t\mathbf{e}_s|},\frac{\nabla\mathbf{F}^t\mathbf{e}_u}{|\nabla\mathbf{F}^t\mathbf{e}_u|}\right].$$

This change of coordinates maps the time-varying stable and unstable directions along the model trajectory $\overline{\mathbf{x}}(t)$ into the two orthogonal directions $(1,0)^T$ and $(0,1)^T$ for all t. The coordinate change gives the transformed system

$$\dot{\mathbf{z}}=\boldsymbol{\Lambda}(t)\mathbf{z}+\mathbf{R}(\mathbf{z},t)+\mathbf{P}(\mathbf{z},t), \tag{B1}$$

with

$$\begin{aligned}\boldsymbol{\Lambda}(t)&=\mathbf{T}^{-1}(t)[\nabla\mathbf{u}(\overline{\mathbf{x}}(t),t)\mathbf{T}(t)-\dot{\mathbf{T}}(t)]\\&=\mathrm{diag}\ (-\lambda_1(t),\ \lambda_2(t)),\end{aligned}$$

where the functions $\lambda_i(t)$ are yet to be determined. The diagonal nature of $\boldsymbol{\Lambda}(t)$ follows from the fact that the subbundles generated by $\nabla\mathbf{F}^t\mathbf{e}_s$ and $\nabla\mathbf{F}^t\mathbf{e}_u$ are invariant under the linearized flow $\nabla\mathbf{F}^t(\mathbf{x}_0)$. The functions $\mathbf{P}$ and $\mathbf{Q}$ are again of the form

$$\mathbf{P}(\mathbf{z},t)=\mathcal{O}(\|\mathbf{T}^{-1}\||\mathbf{T}\mathbf{z}|^2),\quad \mathbf{Q}(\mathbf{z},t)=\mathbf{T}^{-1}\dot{\mathbf{T}}\mathbf{z},$$

and, as in the proof of Theorem 1, satisfy the estimates

$$|\mathbf{P}(\mathbf{z},t)|\leqslant\frac{\sqrt{2}C}{2\alpha}|\mathbf{z}|^2,\quad |\mathbf{Q}(\mathbf{z},t)|\leqslant\frac{\sqrt{2}\beta}{\alpha}|\mathbf{z}|,$$

$$|\mathbf{R}(\mathbf{z},t)|\leqslant\frac{\sqrt{2}}{\alpha}B(t),\quad |\mathbf{R}(\mathbf{z},t)-\mathbf{R}(\overline{\mathbf{z}},t)|\leqslant\frac{\sqrt{2}}{\alpha}L(t)|\mathbf{z}-\overline{\mathbf{z}}|,$$

with

$$\alpha=\min_{t\in I}|\det\mathbf{T}(t)|=\min_{t\in I}\frac{|\det[\nabla\mathbf{F}^t\mathbf{e}_s,\nabla\mathbf{F}^t\mathbf{e}_u]|}{|\nabla\mathbf{F}^t\mathbf{e}_s||\nabla\mathbf{F}^t\mathbf{e}_u|},$$

as defined in (18).

To determine the diagonal elements of $\boldsymbol{\Lambda}(t)$ in (B1), we first note that a direct integration of the linear part of (B1) gives

$$e^{\int_{t_0}^t-\lambda_1(\tau)\,d\tau}=|\nabla\mathbf{F}^t\mathbf{e}_s|=\sqrt{\langle\mathbf{e}_s,\nabla\mathbf{F}^{t*}\nabla\mathbf{F}^t\mathbf{e}_s\rangle},$$

or, equivalently,

$$\begin{aligned}\lambda_1(t)&=-\frac{1}{2}\frac{d}{dt}\log\langle\mathbf{e}_s,\nabla\mathbf{F}^{t*}\nabla\mathbf{F}^t\mathbf{e}_s\rangle\\&=-\frac{1}{2}\frac{\langle\mathbf{e}_s,\nabla\mathbf{F}^{t*}(\nabla\mathbf{u}(\overline{\mathbf{x}}(t),t)^*+\nabla\mathbf{u}(\overline{\mathbf{x}}(t),t))\nabla\mathbf{F}^t\mathbf{e}_s\rangle}{\langle\mathbf{e}_s,\nabla\mathbf{F}^{t*}\nabla\mathbf{F}^t\mathbf{e}_s\rangle}\\&=-\frac{\langle\mathbf{e}_s,\nabla\mathbf{F}^{t*}\mathbf{S}\nabla\mathbf{F}^t\mathbf{e}_s\rangle}{\langle\mathbf{e}_s,\nabla\mathbf{F}^{t*}\nabla\mathbf{F}^t\mathbf{e}_s\rangle},\end{aligned} \tag{B2}$$

just as in (16). The expression for $\lambda_2(t)$ [see (16)] is obtained from a similar calculation.

Under assumption (17), Eq. (B1) satisfies the same assumptions and estimates as Eq. (A2) in the proof of Theorem 1, except that we now have $\beta=0$ since $\mathbf{Q}\equiv\mathbf{0}$. As a result, the statement of the theorem follows from an argument identical to that given in Appendix B.

[1] J. M. Ottino, *The Kinematics of Mixing: Stretching, Chaos, and Transport* (Cambridge University Press, Cambridge, 1989).
[2] G. Haller, "Finding finite-time invariant manifolds in two-dimensional velocity fields," Chaos **10**, 99 (2000).
[3] G. Haller and G. Yuan, "Lagrangian coherent structures and mixing in two-dimensional turbulence," Physica D **147**, 352 (2000).
[4] P. D. Miller, C. K. R. T. Jones, A. M. Rogerson, and L. J. Pratt, "Quantifying transport in numerically generated velocity fields," Physica D **110**, 105 (1997).
[5] A. C. Poje and G. Haller, "Geometry of cross-stream mixing in a double-gyre ocean model," J. Phys. Oceanogr. **29**, 1649 (1999).
[6] K. Bowman, "Manifold geometry and mixing in observed atmospheric flows," preprint (1999).
[7] G. Haller, "Distinguished material surfaces and coherent structures in 3D fluid flows," Physica D **149**, 248 (2001).
[8] C. Coulliette and S. Wiggins, "Intergyre transport in a wind-driven, quasi-geostrophic double gyre: An application of lobe dynamics," Nonlin. Proc. Geophys. **8**, 69 (2001).
[9] G. Lapeyre, B. L. Hua, and B. Legras, "Comments on 'Finding finite-time invariant manifolds in two-dimensional velocity fields,' " Chaos **11**, 427 (2001).
[10] S. Winkler, Ph.D. thesis, Brown University (2001).
[11] G. Haller, "Lagrangian structures and the rate of strain in two-dimensional turbulence," Phys. Fluids **13**, 3365 (2001).
[12] B. Joseph and B. Legras, "On the relation between kinematic boundaries, stirring, and barriers for the Antarctic polar vortex," J. Atmospheric Sci. (to be published).
[13] A. Okubo, "Horizontal dispersion of floatable trajectories in the vicinity of velocity singularities such as convergencies," Deep-Sea Res. Oceanogr. Abstr. **17**, 445 (1970).
[14] J. Weiss, "The dynamics of enstrophy transfer in 2-dimensional hydrodynamics," Physica D **48**, 273 (1991).
[15] R. Doerner, B. Hübinger, W. Martienssen, A. Grossmann, and S. Thomae, "Stable manifolds and predictability in dynamical systems," Chaos, Solitons, Fractals **10**, 1759 (1999).
[16] R. T. Pierrehumbert, "Large-scale horizontal mixing in planetary atmospheres," Phys. Fluids A **3**, 1250 (1991).
[17] R. T. Pierrehumbert and H. Yang, "Global chaotic mixing on isentropic surfaces," J. Atmos. Sci. **50**, 2462 (1993).
[18] D. Elhmaïdi, A. Provenzale, and A. Babiano, "Elementary topology of two-dimensional turbulence from a Lagrangian viewpoint and single-particle dispersion," J. Fluid Mech. **257**, 533 (1993).
[19] J. von Hardenberg, K. Fraedrich, F. Lunkeit, and A. Provenzale, "Transient chaotic mixing during a baroclinic life cycle," Chaos **10**, 122 (2000).
[20] N. Malhotra, I. Mezić, and S. Wiggins, "Patchiness: A new diagnostic for Lagrangian trajectory analysis in time-dependent fluid flows," Int. J. Bifurcation Chaos Appl. Sci. Eng. **8**, 1053 (1998).